

# Redesign of Industrial Apparatus Using Multi-Objective Bayesian Optimisation

S.J. Daniels\*, A.A.M. Rahat, R.M. Everson, G.R. Tabor, J.E. Fieldsend  
Corresponding author: S.Daniels@exeter.ac.uk

\*CEMPS, University of Exeter, UK.

**Abstract:** In this paper, a two-dimensional cross-flow tube-bundle heat exchanger arrangement problem with internal laminar flow is considered. multi-objective optimisation was performed with a recently developed Bayesian approach. The parameters of the tube configuration include the streamwise-position, number, and radii of tubes. The goal was to find a range of geometries that optimally trade-off the rate of heat exchange and the pressure loss. A systematic study was performed involving 400 Computational Fluid Dynamic (CFD) evaluations. A fully automated in-house python-based framework was used to solve the problem, including mesh generation and CFD simulation. The main purpose of this article is to illustrate and analyse a heat exchanger tube arrangement problem in its most general form, and to provide a fundamental understanding of the structure of the Pareto front and optimal geometries. The considered conditions are particularly suited for low-power applications, as found in a growing number of practical systems in an effort toward increasing energy efficiency.

*Keywords:* Heat exchanger, Tube bundle, Unequal tube diameters, Tube pitch ratios, Multi-objective optimisation, Bayesian optimisation.

## 1 Introduction

A cross-flow tube-bundle heat exchanger is one of the simplest but most effective apparatus for heat transfer applications. Their range of size allows for a wide variety of applications in many fields, such as the chemical, food and nuclear industries, and HVAC (Heating, Ventilation and Air Conditioning) sectors, to name a few. Generally, this type of heat exchanger contains many rows of tubes oriented in a direction perpendicular to the flow, as shown in Fig.1. The tubes may be arranged in many configurations in order to obtain the greatest heat transfer between the two media. The transfer of heat between the tubes and the main flow occurs through the tube walls and will be maximised by increasing the surface area of contact between the flow and the walls. A detrimental effect of this may be that the static pressure across the tube configuration increases, requiring greater energy (pumping power) to push the flow through the heat exchanger. Overall, this potentially results in a conflicting pair of objectives for its design. The resulting problem is a multi-objective task involving, at least, two conflicting goals: in this case, no one solution can be usually judged the best with respect to all the objectives, but a set of trade-off optimal solutions must be considered. The ensemble of these compromise solutions constitutes the so called Pareto front. To reduce the computational cost, it is common practice (e.g. [1, 2]) to transform the multi-objective problem into a single objective one, by incorporating all the objectives into a single function with the use of arbitrary weighting factors. However, this strategy is not always advisable, since it does not give access to the whole set of optimal solutions, and the results strongly depend on the chosen weighting factors [3].

Optimisation of a tube-bundle heat exchanger may be pursued by a number of active and passive methods. Active methods aim to control the flow by providing external energy, while passive methods focus on altering the geometry of the tube bundle by changing the tube arrangement, tube diameters and relative pitches. One suggested active method is to superimpose pulsations on the inflow, leading to vortex shedding lock-on

in an in-line [4] or semi-staggered [5] tube bundle arrangement, and therefore heat transfer enhancement. However, any benefits should be offset against the power required to generate the pulsations. Similarly, changing the turbulent regime of the flow may provide an enhancement in heat transfer, for example, Taub [6] found that increasing the turbulence intensity resulted in this effect.

Despite the significant number of publications on optimising the heat exchanger design, three main gaps have not been fulfilled. Firstly, the design spaces investigated comprise of a low number of design variables within limited ranges; most studies consider fixed number of tubes (rows) and/or tube pitch ratios. Second, the investigations are usually limited to simple parametric analysis on the fluid flow only. Utilising a robust approach (e.g. Design Of Experiment [7]) would allow for a larger number of design variable combinations, thus providing better mapping for the thermal-hydraulic performance changes within the design space. Finally, all studies treat the tube-bundle on a qualitative basis i.e. only the topology variables (pitch ratios) are accounted in addition to Reynolds numbers.

For practical engineering applications of optimal shape design, coupling an optimisation algorithm with CFD in an automated procedure has become increasingly popular in the literature. In the context of the tube-bundle heat exchanger, the majority of papers focus on the optimisation of the tube shapes or positions. Bejan and Fowler [8] performed a theoretical, numerical and experimental study for selecting the best spacing between horizontal pipes in a fixed volume subjected to natural convection, in order to maximise heat transfer (Single-Objective). A similar configuration was considered by Stanescu et al. [9]. The maximisation of the heat transfer rate under a volume constraint was achieved also by Matos et al. [10]. In their geometric optimisation they considered both circular and elliptic tubes to describe more general configurations; their work was extended to a three-dimensional domain in [11, 12]. Hilbert et al. [13] performed a multi-objective optimisation using a Genetic Algorithms (GAs) on elliptical and blade/tear-drop cross-sections of the tubes in a staggered formation. Similar work has also been performed by Ranut et al. [14] focusing on the elliptical pipe cross-section while comparing the efficacy of the NSGA-II and FMOGA-II genetic algorithm. It should be noted however, that the manufacture of elliptic or blade/tear-drop pipes may prove to be problematic. A simpler alternative is to optimise the formation of the circular pipe; papers such as Daroczy et al. [15] and Ge et al. [16] applied the NSGA-II Algorithm to perform such analysis. Overall, it should be noted from the papers listed above that the number of CFD evaluations required when using GAs are  $\sim \mathcal{O}1000$ , making this costly investigation. Developing an efficient, robust and accurate multi-objective optimisation technique for such problems involving complex geometries, flow and heat transfer in a coupled manner, would be extremely important for future applications.

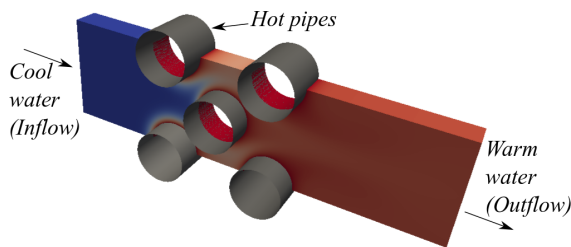


Figure 1: A demonstration of a staggered formation of the cross-flow tube-bundle heat exchanger.

An improvement to the GA is to adopt a surrogate modelling approach, reducing the number of evaluations down to  $\sim \mathcal{O}100$ . To the best of the authors' knowledge, in the literature, the application of a surrogate-based optimisation procedure has not yet been applied to the multi-objective optimisation of a tube-bundle heat exchanger. Furthermore, the authors' are not aware of any automated optimisation procedure of the tube bundle, with design variables such as position, radii and number of pipes per column. Moreover, it should also be of interest to the reader that the tube-bundle configuration shares similar thermal-hydraulic properties to that of the plain fin-and-tube heat exchanger (see [17]). Overall, the present work aims to address the following topics:

1. To systematically carry out the multi-objective optimisation of a cross-flow tube bundle heat exchanger, with design variables of radii, number, and pitch ratios of the pipes.
2. To apply a newly developed Bayesian optimisation method for solving multi-objective problems.

## 1.1 Paper Overview

In the present work, multi-objective optimisation of a tube-bundle heat exchanger by means of Bayesian Optimisation is carried out. The design consideration for the tube configuration include the number, radii, and streamwise position. The structure of this paper is as follows: firstly, the tube bank configuration, design parameters, and working conditions are outlined - this is closely followed by the numerical setup for CFD; secondly, the method of mesh perturbation for each design is outlined with a mesh convergence study; thirdly, the optimisation strategy is outlined, beginning with the design objectives, design representation, and the multi-objective Bayesian methodology is described; Finally, the results of the optimisation simulations are presented with phenomenological discussion and conclusion.

## 2 Numerical methodology for CFD

### 2.1 Tube bank heat exchanger configuration

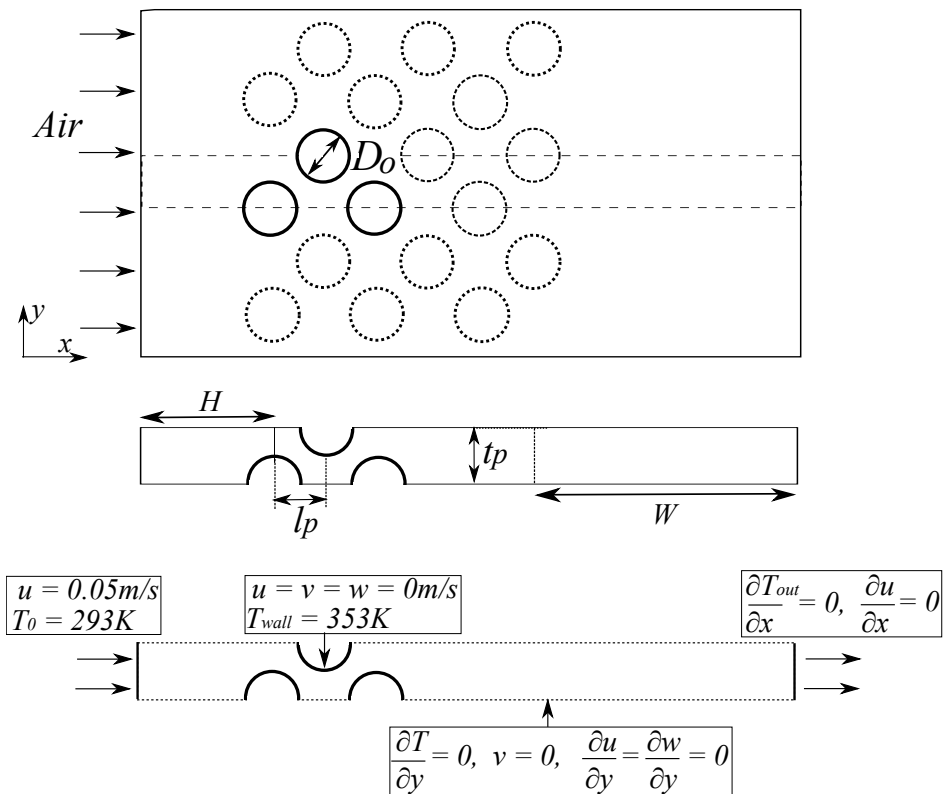


Figure 2: Top: Cross-section in  $y - x$  plane: the tubes are in staggered arrangement; middle: schematic of the CFD domain with labelled dimensions for the pipe configurations and optimisation space; bottom: schematic of the boundary conditions around the CFD domain.

A tube-bundle heat exchanger with the pipes in a staggered arrangement was constructed using the open-source C++ code OpenFOAM-4.x. The flow pattern is assumed to be repeated between from one row to the next - regardless of an in-line or staggered tube array. Based on this assumption (and the flow assumptions outlined below), it is speculated that only one period of arrays is needed for the solution of the flowfield [18]. It should be noted that the configuration of the pipes during the optimisation process may result in an alternating fluid flow depending on the considered number of columns. In the present work, two column arrays are considered, as shown in Fig.5. It has already been shown in the literature that maximum efficiency is achieved with a symmetrical configuration of tubes [15]. The diameter of the ‘base’ tube,  $D_0 = 0.01\text{m}$ . Air

enters the domain from the left with  $T_0 = 293K$  and is warmed up by passing between tubes in which a warm fluid flows in the corresponding application. A no-slip condition, and a constant uniform temperature are imposed on the tube walls, with  $T_{wall} = 353K$ . A uniform inflow is imposed with  $u = 0.05m/s$ . Symmetry conditions were applied to the upper and lower boundaries of the domain. A pressure-outlet with ambient pressure and zero-gradient velocity are applied at the outflow. The total streamwise length of the CFD domain is  $12D_0$  with a wake region,  $W$ , set to  $4.75D_0$  to avoid any backflow and to ensure convergence of the CFD solution.

On the fundamental side, the heat transfer and fluid flow over the tube bundles has been the subject of many papers, either through original experimental work ([19, 20]), as well as very recent high-level numerical studies focusing on the unsteady flow phenomena and turbulence ([21, 22]). In the present work, the inspiration for the design parameters for optimisation will be from the configurations typically observed in the literature.

According to Zukauskas and Ulinskas [23], tube banks with  $t_p \times l_p \leq 2.5D_0 \times 1.25D_0$  are considered compact, and with  $t_p \times l_p \geq 4D_0 \times 2D_0$  are classed as widely spaced. Using a simplified model, Kahn et al. [24] derived a series of analytical expressions for the heat transfer of both in-line and staggered arrangements of tubes, and subsequently investigated the effects of varying the pitch ratios ( $t_p/l_p$ ). It was found that for both staggered and in-line arrangements, the heat transfer increases mainly with decreasing longitudinal pitch ratio, and to a lesser extent with increasing transverse pitch ratio. Compact banks (in-line or staggered) indicate higher heat transfer rates than widely spaced ones. For the same pitch ratio, the heat transfer is higher in a staggered bank than for an in-line tube bank. This was due to the fact that in a staggered bank, the path of the main flow is more complicated and a greater portion of the surface area of downstream tubes remains in this path. The effects of the tube arrangement of the frictional losses (pressure drop) were not considered in their work. In the present work, the optimisation process would allow for the variation of  $l_p$  between the pipes as a design variable. The transverse pitch,  $t_p$ , on the other hand, will be fixed with  $t_p = 2D_0$  to allow for the analysis of the widely-spaced heat exchanger. This, combined with the varying pipe diameters, allows for the consideration of a compact tube bundle. The longitudinal distances between the pipes can be varied between  $(D_1/2 + D_2/2)/\Delta x \leq l_p \leq 5D_0$ , where  $\Delta x$  is the distance between the center points of two adjacent pipes along the same column. Furthermore, regardless of longitudinal pitch, it has also been demonstrated in the literature that there is little improvement in heat transfer for number of pipes greater than 3 per column in laminar flow (e.g. [25]) - though increasing this number may significantly affect the pressure drop. Therefore, for the present work, the maximum number of pipes per column was conservatively limited to 3.

Typically, in the literature, experimental and numerical works involving tube bundles are performed with tube diameters of  $0.01 - 0.051m$ . Only recently have tube bundles with a smaller diameters been of interest (e.g.  $0.0015m$ , [26]), since mini-channel tubes provide a higher compactness for a low Reynolds number operation range. Moreover, compared to the effects of pitch ratios, tube bundles consisting of multiple pipe diameters are also a recent contribution to the literature (e.g. [27]). Of these investigations, a number of researchers have found that installing a pipe upstream or downstream of a larger one is able to significantly affect the wake flow (and subsequently the pressure recovery across the apparatus). Although not all the aforementioned studies are directly applicable to tube bundle heat exchangers, they do indicate the beneficial effects from the use of unequally sized pipe arrangements for suppressing flow activity in tube wakes. Using a Design Of Experiment framework, Bacellar et al. [7] investigated the effects of varying tube diameter ( $0.0005m \leq D \leq 0.002m$ ), pitch ratios ( $1.2 \leq t_p/D, t_p/D \leq 4$ ) in a staggered arrangement, and inflow air velocity. Their correlation results show potentially that despite reducing the tube diameter, the same heat capacity may be achieved to that for the heat exchanger consisting of larger tube sizes. Mavridou et al. [28, 27] conducted the numerical and experimental analysis of pairs of in-line cylinders with unequally sized tubes ( $D = 0.00635m$  and  $0.0127m$ ) and various pitch ratios ( $l_p/D = 1.5D, 3.6D$  and  $t_p/D = 2.5D, 3.6D$ ); their results showed that compared to a conventional staggered tube bundle (constant diameters), the arrangement with the smaller diameter upstream of the larger one in an in-line arrangement had a significant increase in heat transfer; the equivalent arrangement with a smaller transverse distance ( $t_p$ ) increased the heat transfer significantly but at an expense of an increase in pressure drop. It should be noted that sourcing the small diameter tubes for practical use is a challenging endeavour. Therefore, the diameter ranges chosen for the present work will be of a conservative range for a tube-bundle heat exchanger typically observed in the literature (e.g. [27]), with  $0.005m \leq D \leq 0.025m$ .

In summary, for the design space, the chosen ranges of pipe diameter ( $D$ ), streamwise positions ( $x_c$  being the center of the pipes), and number of pipes ( $N$ ) are prescribed:

$$0.5D_0 \leq D \leq 2.5D_0; \quad (1)$$

$$2.25D_0 \leq x_c \leq 7.25D_0; \quad (2)$$

$$N \in \mathbb{N}[1, 3]. \quad (3)$$

## 2.2 Governing equations

The Reynolds number of the air flow across the heat exchanger is defined as

$$Re = \frac{\rho u D_{max}}{\mu} = 39.0625 < Re_1 \quad (4)$$

where  $u$  is the inflow velocity,  $D_{max}$  is the maximum diameter of the pipes considered in this work,  $\rho$  and  $\mu$  are the density and dynamic viscosity of the flow medium. The reference Reynolds number  $Re_1 = 46$  according to Barkley and Henderson [29], or  $Re_1 = 47 \pm 1$  following Norberg [30]. Above this value, the fluid undergoes a supercritical Hopf-bifurcation leading to a periodic, oscillatory flow. However, in the present case, the Reynolds number is well below this limit. Therefore, a laminar and steady flow can be safely assumed, as done in all simulations. For flow past a stationary cylinder, three-dimensional instabilities occur first at around  $Re = 189$  and  $Re = 259$  (Mode A and Mode B, respectively [29]). Therefore, three-dimensional simulations were not required in the present case, and only a two-dimensional slice across of the heat exchanger will only be simulated in what follows. Gravity is also not included in the CFD simulation. The effects of buoyancy is neglected as well, since only a small density change will be expected in the temperature range. The working fluid (air) across the heat exchanger is considered to be incompressible (i.e. Mach number is low), steady, and two-dimensional as described above. The air flow through the cross-flow pipes is assumed to be at a high velocity, resulting in a constant tube-surface temperature (isothermal); the thermal radiation (i.e. temperatures are not considerably high), and viscous dissipation and work are neglected. Under these assumptions, the governing equations of the fluid are described,

Continuity:

$$\frac{\partial u_i}{\partial x_i} = 0, \quad (5)$$

Conservation of momentum:

$$\frac{\partial u_i u_j}{\partial x_j} = -\frac{1}{\rho} \left( \frac{\partial p}{\partial x_i} \right) + \frac{\mu}{\rho} \frac{\partial^2 u_i}{\partial x_j \partial x_j}. \quad (6)$$

where  $u$  is the velocity vector,  $p$  is the static pressure, and index  $i = 1, 2, 3$  or  $x, y, z$ . Equations 5 and 6 are solved along with the steady state equation for the energy balance, described:

$$c_p \rho \frac{\partial u_j T}{\partial x_j} = k \frac{\partial^2 T}{\partial x_j^2} \quad (7)$$

where  $T$  is the static temperature,  $c_p$  is the specific heat capacity at constant pressure, and  $k$  is the thermal conductivity of the fluid. The Finite Volume Method was employed to integrate the governing equations by transforming the volume integration into surface integration for each control volume [31]. The second-order central difference scheme was used to discretise the diffusion terms, and the second-order upwind difference was adopted to approximate the convection term. The SIMPLE algorithm [32] was used for the pressure-velocity coupling, with under-relaxation factors 0.7, and 1 for the velocity, and pressure respectively. All simulations were run with prescribed residual limits of  $10^{-6}$ ,  $10^{-7}$ , and  $10^{-8}$  for momentum, pressure, and temperature flow variables. The maximum number of iterations was set to 8000; convergence was always achieved within this duration. The generalised Geometric-Algebraic Multi-Grid solver was used for pressure, while the Gauss-Seidel linear solver was used for the remaining fields. Due to the small range of temperatures

involved in this problem, the material properties of the air flow across the domain are regarded as constants:

$$c_p = 1006.5 \frac{J}{Kg.K}; \quad k = 0.026341 \frac{W}{m.K}; \quad \rho = 1.1649 \frac{Kg}{m^3}; \quad \mu = 1.868 \times 10^{-5} \frac{Kg}{m.s}. \quad (8)$$

### 2.3 Objective Functions

The obvious goal is to maximise the efficiency of the heat exchanger. However, this goal cannot be mathematically formulated as a single value or indicator; at least two objectives are needed, which are known from many previous works as being concurrent. On the one hand, the pressure loss (which is proportional to the power needed) is to be minimised. The friction factor,  $f$ , a ratio of wall shear stress to the flow kinetic energy, represents the pressure drop for heat exchangers, described,

$$f = \frac{1}{\frac{1}{2}\rho u_{in}^2} \left[ \frac{1}{A_{out}} \int_{A_{out}} p_{out} dA_{out} - \frac{1}{A_{in}} \int_{A_{in}} p_{in} dA_{in} \right], \quad (9)$$

where  $p$  is the static pressure along the boundary, and  $u$  is the streamwise velocity component,  $A$  is the cross-sectional area, and subscripts *in* and *out* indicate the inflow and outflow boundaries of the domain. Alternative cost functions in the literature representing the pressure loss include the power input per unit volume [33], a modified friction factor including the maximum local velocity or area ratios between the pipes and domain [34], normalised hydraulic resistance [35], or, quite simply, the pressure drop alone [13, 36, 14].

The second objective is related to the efficiency of the heat transfer process. Several different metrics have been proposed in the literature for this quantity, e.g. temperature difference between outlet and inlet [13, 14], Nusselt number [35, 37], entropy resistance [38], thermal resistance [39], entropy generation number [35, 40], total heat transfer [33, 15] or mean heat transfer coefficient [33].

In the present problem, the total heat transfer can be formulated along the outflow boundary as

$$\dot{Q} = \rho c_p \int_{A_{out}} (T_{out} - T_0) u_{out} dA_{out}, \quad (10)$$

By substituting the constant wall temperature as  $T_{out}$  and assuming the velocity across the apparatus is left unperturbed, the maximum possible value for total heat transfer,  $\dot{Q}_{max}$ , is obtained. For a more straightforward comparison, the theoretical efficiency of the heat exchanger,  $\eta$ , is introduced which can be calculated as  $\eta = \dot{Q}/\dot{Q}_{max}$ , and is non-dimensional. The value of  $\eta$  is to be maximised, with a value range of  $\eta \in [0, 1]$ .

### 2.4 Automated mesh regeneration

The optimisation process takes place in a fully automated manner, using a python-based framework<sup>1</sup> (detailed in [41]). From the CFD side, in the present work, the automated procedure includes geometry creation, hybrid mesh generation, and CFD evaluation. A meaningful design optimisation study demands a consistency in numerical accuracy. As a consequence, an appropriate emphasis must be on the mesh quality for each evaluation. However, when evaluating hundreds of designs, case-by-case dedication to the construction of structured meshes is unfeasible. High-quality, but automatic meshing is required, for which unstructured (or hybrid) meshes are recommended.

In the present work, for the purpose of automating the meshing process for each evaluation, the utility `snappyHexMesh`, available in `OpenFOAM-4.x`, was utilised. To use `snappyHexMesh`, the user provides an stereolithography (STL) file of the geometry and a base mesh (typically a simple hexagonal block-structured mesh). `SnappyHexMesh` then operates a three-stage meshing process of castellation, snapping and boundary layer refinement. In the first step (castellation), cells are identified which are intersected by edges of the surface geometry; these cells are then refined by repeated cell splitting, with maximum and minimum levels of refinement being a definable parameter, and further surface refinement also being controllable. After this refinement process, all cells which lie ‘outside’ the desired geometric domain are deleted from the mesh (for a bluff body, this would be cells on the interior of the STL geometry). In the second, snapping step, vertices

<sup>1</sup>Python code for the CFD framework is available at: <http://bitbucket.org/arahat/cfd-test-problem-suite/>

on the edge of the domain are ‘snapped’ to the STL surface, using an iterative process of mesh movement, cell refinement and face merging, again controlled by user-defined parameters such as number of iterations and specific mesh quality constraints. In a final and optional step, cell layers can be added to the surface to move the mesh away from the boundary to specifically refine a boundary layer. The whole process is robust and automated, but is controlled by a large number of user-specified parameters provided in advance as an input file. As with any meshing process, the user typically has to experiment with different settings to optimise the mesh quality. Mesh quality may ultimately be judged by the success of the resulting CFD run, but as a proxy various mesh quality indicators such as skewness and non-orthogonality can more easily be evaluated. The entire process can be constrained by the overall number of cells, both locally in the boundary layer, or the entire domain.

In the first step a mesh independence study was performed for different mesh sizes and for a chosen feasible design. The pipe configuration chosen for this study consists of 2 pipes per column in a staggered formation. The vertical ( $t_p$ ) and horizontal ( $l_p$ ) distances between the centers of the pipes were set to  $2D_0$ . the diameters of the pipes were chosen to be  $D_0$ . The focus for mesh refinement was of the base (structured hexagonal) mesh. The mesh was refined by either doubling or halving the number of cells on the streamwise and vertical directions ( $x, y$ ), while maintaining an aspect ratio of 1. Based on the earlier grid-sensitivity study by Rajani et al. [42], all the present calculations maintain a wall-normal distance of the first internal grid point of  $\Delta r = 0.0001D_0$  ( $r$  is the radius), as recommended by Rajani et al. [43] to capture the sharp near-wall gradients of the flow variables; the number of layers specified for the boundary layer was set to 25, with a growth rate of 1.15. It should be noted that in equivalent studies, (e.g. [15]) a fully unstructured mesh may only be the viable option when considering the vast number of CFD simulations. Daroczy et al. [15] studied the sensitivity of the cost functions (also used in the present work) to a block-structured and unstructured mesh. Their results indicate very little sensitivity for the total heat transfer  $\eta$  with decreasing cell size and mesh formation; the friction losses, on the other hand, showed considerable changes that the mesh formation - convergence was achieved with a lower number of cells for the structured mesh than the equivalent unstructured.

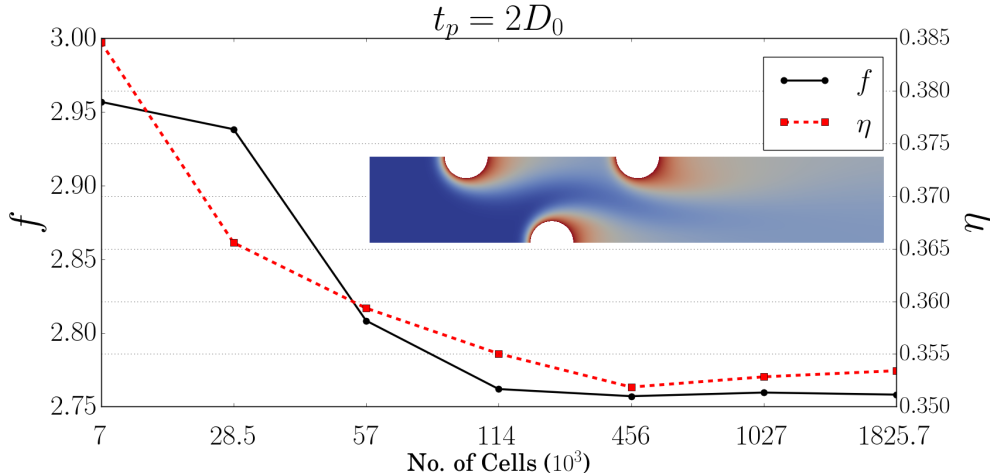


Figure 3: Mesh-independency test concerning the hydraulic resistance and total heat transfer.

Corresponding results of the cost functions in the present work to the average mesh size generated from the resulting snappyHexMesh (hybrid) mesh is shown in Fig.3. The  $x$ -axis reports the total number of cells after the castellation, snapping, and layer process of snappyHexMesh. As it can be seen for both cost functions that with increasing the number of cells in the mesh, convergence is achieved at the same number of grid points. Convergence was achieved at a lower number of cells to that reported in Daroczy et al. [15] due to the use of a block-structured cell distribution towards the outflow. Thus the block structured mesh for 456,000 cell case was used for the optimisation run with the boundary layer characteristics described above. The corresponding cell size,  $\Delta$ , was equal to  $\Delta/t_p = 10^{-4}$ , with aspect ratio  $\Delta_x/\Delta_y = 1$ .

### 3 Numerical Representation for Shapes

#### 3.1 Chebyshev Polynomials

Often multiple geometric variables may be spatially related, but the nature of this relationship may not be known *a priori*. Rather than representing these independently, it may be useful to encode their relationship with a parametrised function such that altering the parameters changes all geometric variables simultaneously. An additional benefit is that a small number of parameters may then represent a large number of variables, and consequently reduce the search space size. In this paper, Chebyshev polynomials [44] were used for encoding spatial relationships for one dimensional variables, in particular the radii and the number of pipes.

A function based on Chebyshev polynomials (type I) may be defined as:

$$f(t, \mathbf{c}) = \sum_{i=0}^n c_i T_i(t), \quad (11)$$

where,  $t \in [0, 1]$  is a location variable, the  $i$ th basis function is  $T_i(t) = \frac{(-2)^i i!}{(2i)!} \sqrt{1-x^2} \frac{d^i}{dx^i} (1-x^2)^{\frac{i-1}{2}}$ , and the associated coefficient vector  $\mathbf{c} = (c_1, \dots, c_n)^\top$  with  $c_i \in [-1, 1]$ . With this parameterised function, if there are  $k$  variables at locations  $t_1, \dots, t_k$ , and a vector of  $n$  coefficients (or parameters)  $\mathbf{c}$ , then the  $j$ th variable of interest takes the value:

$$v_j = f(t_j, \mathbf{c}). \quad (12)$$

The coefficient vector may be directly considered as the decision vector here, and as it is varied, a distinct value for  $v_j$  at a fixed location  $t_j$  may be achieved.

Note that it is straightforward to scale the variables  $v_j$  and locations  $t_j$  between specified lower and upper bounds. Furthermore, so long as  $n < k$ , a smaller number of coefficients (or parameters) in this representation may directly encapsulate and control the relationships between the  $k$  variables  $v_1, \dots, v_k$ . Thus this may effectively reduce the search space. An illustration of the scheme is presented in Fig.4a.

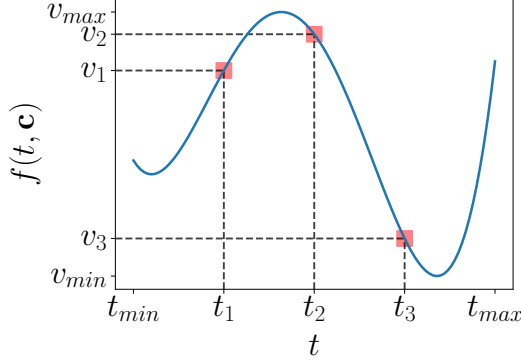
#### 3.2 Monotonic Beta Cumulative Distribution Functions

It can be envisaged that some geometric variables may be monotonically increasing with respect to a location. Again, parametric monotonic functions may be used to encode such relationships. In this paper, a weighted sum of cumulative distribution functions (CDFs) of Beta distributions was used for this purpose, which is a suitable representation for the centres of the pipes.

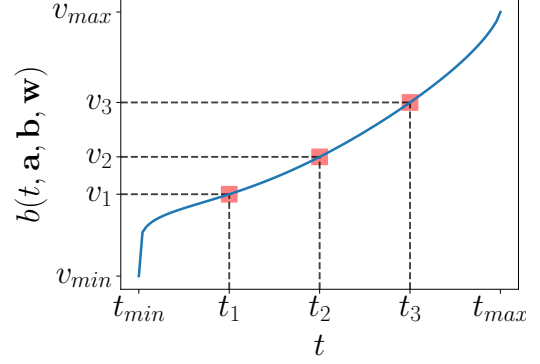
Let the function  $F(t, \alpha, \beta)$  be the CDF of a Beta distribution. The CDF monotonically increases from zero to one as location  $t$  is changed from zero to one for a specified set of shape parameters  $\alpha > 0$  and  $\beta > 0$ . If the shape parameters are altered to  $\alpha'$  and  $\beta'$ , this will result in a distinct monotonic relationship between  $t$  and  $F(t, \alpha', \beta')$  in comparison to  $t$  and  $F(t, \alpha, \beta)$ . To further increase the flexibility of such a representation, the weighted sum of multiple Beta CDFs may be considered, and as a convex combination of monotonic functions this will preserve the monotonicity. Such a combination of  $n$  Beta CDFs may be expressed as:

$$b(t, \mathbf{a}, \mathbf{b}, \mathbf{w}) = \sum_{i=1}^n \omega_i F(t, \alpha_i, \beta_i), \quad (13)$$

where  $\mathbf{w} = (\omega_1, \dots, \omega_n)^\top$  is the weight vector with  $\sum_i \omega_i = 1$ , and  $\mathbf{a} = (\alpha_1, \dots, \alpha_n)^\top$  and  $\mathbf{b} = (\beta_1, \dots, \beta_n)^\top$  are the vectors of parameters for the Beta distribution. As in section 3.1, the monotonic variable of interest can now be computed using Eq.(12) by replacing  $f(t_j, \mathbf{c})$  with  $b(t, \mathbf{a}, \mathbf{b}, \mathbf{w})$ . Again, if a small  $n$  number of Beta functions is chosen to represent a large  $k$  number of monotonic geometric variables, then this would efficiently reduce the size of the search space. The scheme is depicted in Fig.4b.



(a) Chebyshev polynomials from (11).



(b) Monotonic Beta CDF from (13).

Figure 4: Illustration of parametric functions: Chebyshev polynomials in (a) and monotonic Beta CDFs in (b). The function responses are depicted in blue. The red squares show the selected function values  $v_1, v_2$  and  $v_3$  at locations  $t_1, t_2$  and  $t_3$ . The locations were scaled between  $t_{min}$  and  $t_{max}$ , and the values were scaled between  $v_{min}$  and  $v_{max}$ . Here, arbitrary parameter vectors  $\mathbf{c}, \mathbf{a}, \mathbf{b}$  and  $\mathbf{w}$  were chosen for demonstration. Clearly, changing the parameters will result in a different function response. Thus, a variable of interest  $v_j$  at a fixed location  $t_j$  may be varied by changing the relevant parameters.

## 4 Multi-objective shape optimisation

In this paper, the primary goal is to simultaneously minimise the pressure drop and maximise the total heat transfer. Consider that a particular heat exchanger geometry may be represented with an  $n$ -dimensional decision vector  $\mathbf{d} \in \mathcal{D}$ , where  $\mathcal{D} \in \mathbb{R}^n$  consists of all feasible shapes. For each row, a two-coefficient Chebyshev function for radii, a two-coefficient Chebyshev function for the number of pipes and two-Beta CDFs for the centres of the pipes were used. This resulted in an 18 dimensional decision vector. With this, the multi-objective optimisation problem may be expressed as:

$$\min_{\mathbf{d} \in \mathcal{D}} f_1(\mathbf{d}) = f, \quad (14)$$

$$\min_{\mathbf{d} \in \mathcal{D}} f_2(\mathbf{d}) = -\eta. \quad (15)$$

The objectives are highly conflicting. As such, generally there is not a unique solution to this problem, but a range of shapes that trade-off between the objectives. The trade-off relationship is characterised by the notion of dominance [45]. A shape  $\mathbf{d}$  is said to dominate another shape  $\mathbf{d}'$ , denoted as  $\mathbf{d} \prec \mathbf{d}'$ , if,

$$\begin{aligned} & f_1(\mathbf{d}) < f_1(\mathbf{d}') \text{ and } f_2(\mathbf{d}) \leq f_2(\mathbf{d}') \\ \text{or } & f_1(\mathbf{d}) \leq f_1(\mathbf{d}') \text{ and } f_2(\mathbf{d}) < f_2(\mathbf{d}'). \end{aligned} \quad (16)$$

The set of shapes that optimally trade-off between the objectives is referred to as the Pareto set:

$$\mathcal{P} = \{\mathbf{d} \mid \mathbf{d}' \not\prec \mathbf{d} \forall \mathbf{d}', \mathbf{d}' \in \mathcal{D} \wedge \mathbf{d} \neq \mathbf{d}'\}. \quad (17)$$

It may not be possible to locate the exact Pareto set within a practical time limit, even if the objective functions were computationally cheap. Therefore, the overall goal of an effective optimisation approach is to generate a good approximation of the Pareto set denoted as  $\mathcal{P}^* \subseteq \mathcal{D}$ .

Multi-objective Bayesian optimisation (MBO) is a surrogate model based global search strategy that sequentially samples the design space at likely locations of shapes which may improve the current approximation of the Pareto set. One approach towards MBO is to reduce (or scalarise) the multi-objective problem into a single objective problem [46]. This enables the use of standard single objective Bayesian optimisation method in which a data-driven stochastic model (usually a Gaussian process model) is constructed, and then the prediction from the model is used to locate promising solutions [47].

To ensure that sequential sampling improves the current approximation of the Pareto set  $\mathcal{P}^*$ , the formulation of scalarisation function may be relative to the quality of the  $\mathcal{P}^*$  [46]. In this paper, the hypervolume [48] – a set based indicator that measures the objective space covered between a non-dominated set and a predefined reference vector – is used as a quality measure for the  $\mathcal{P}^*$ . It is an exceptional indicator as maximising it is equivalent to locating the optimal Pareto set [49]. The details of the MBO approach with this scalarisation technique is given in [46], but a brief description of the method is provided below for completeness.

MBO starts with a space filling design (e.g. Latin Hypercube Sampling [50]) of the feasible design space. The initial set of  $M$  feasible shapes  $D = \{\mathbf{d}^1, \dots, \mathbf{d}^M\}$  are then expensively evaluated with appropriate CFD simulations, and this provides a data set  $S = \{(\mathbf{d}^m, f_1(\mathbf{d}^m), f_2(\mathbf{d}^m))\}_{m=1}^M$ . Thus an initial approximation of the Pareto set  $\mathcal{P}^* = \text{nondom}(S)$  using (17) may be made. The hypervolume improvement scalarisation  $g(\mathbf{d}, \mathcal{P}^*)$  for all  $\mathbf{d} \in D$  is then applied on the data set  $S$  generating  $\bar{S} = \{(\mathbf{d}^m, g(\mathbf{d}^m, \mathcal{P}^*))\}_{m=1}^M$ . Using this set of the initial shapes and the associated hypervolume improvement  $\bar{S}$  as the training data a stochastic regression model is constructed with a Gaussian process ( $\mathcal{GP}$ ).

The predictive density from the  $\mathcal{GP}$  model for a shape  $\mathbf{d}$  is:  $p(\hat{g}(\mathbf{d})|\bar{S})$ . This enables the closed form calculation of a utility function: the expected improvement in function value (with respect to the best function value observed so far) to be obtained by querying a solution. Given the best evaluated shape  $\mathbf{d}^* = g(\mathbf{d}^*, \mathcal{P}^*) \in \bar{S}$ , the expected improvement of an arbitrary feasible shape  $\mathbf{d}'$  is defined as:

$$\alpha(\mathbf{d}', \mathbf{d}^*) = \int_{-\infty}^{\infty} \max(\hat{g}(\mathbf{d}') - g(\mathbf{d}^*, \mathcal{P}^*), 0) p(\hat{g}(\mathbf{d})|\bar{S}) d\hat{g}(\mathbf{d}). \quad (18)$$

As the predictive distribution is Gaussian, this integral can be calculated in closed form. Thus, selecting the next shape to evaluate is the solution of the following sub-problem:  $\mathbf{d}^{M+1} = \arg\max_{\mathbf{d} \in \mathcal{D}} \alpha(\mathbf{d}, \mathbf{d}^*)$ . Bi-POP-CMA-ES was used to locate a good approximation of the optimum in the sub-problem [51]. The data set  $S$  is then augmented with the newly evaluated shape  $S \leftarrow S \cup \{(\mathbf{d}^{M+1}, f_1(\mathbf{d}^{M+1}), f_2(\mathbf{d}^{M+1}))\}$ , and the current approximation for the Pareto set is updated  $\mathcal{P}^* \leftarrow \{\mathbf{d} | \mathbf{d} \not\prec \mathbf{d}' \wedge \mathbf{d} \neq \mathbf{d}' \forall \mathbf{d}, \mathbf{d}' \in D\}$ . With this, the training data is updated  $\bar{S} \leftarrow \bar{S} \cup \{(\mathbf{d}^{M+1}, g(\mathbf{d}^{M+1}, \mathcal{P}^*))\}$  and the model is retrained. In this process, when the limit on the number of expensive function evaluations is reached,  $\mathcal{P}^*$ , i.e. the current approximation of the Pareto set is returned. A single design from  $\mathcal{P}^*$  may then be selected by the decision maker based on desired performance level.

## 5 Results

The MBO proposed in [46] was used to generate the results in this paper<sup>2</sup>. The optimiser requires a few parameters to be set *a priori*. These settings are discussed below.

Firstly, it is essential to set the number of initial evaluations, so that a surrogate model may be constructed. Traditionally, this is set to  $M = 11n - 1$ , where  $n$  is the number of dimensions in the decision vector  $\mathbf{d}$  [52]. Here,  $n = 18$  and thus the number of initial samples were set to 197. Usually a set of lower and upper limits are also set to enable Latin hypercube sampling and generate initial set of decision vectors  $D = \{\mathbf{d}^1, \dots, \mathbf{d}^M\}$ . Here, additional constraints were imposed to avoid overlapping of the pipes. The pipes are also constrained to tranverse between the distance  $H$  downstream of the inflow, and  $W$  upstream from the outflow. Thus, any Latin hypercube samples that violated these constraints were rejected. As a consequence, only 126 out of 197 initial samples were deemed feasible recasting  $M = 126$ . These  $M$  feasible shapes were evaluated using CFD to acquire the function values and construct the training data set  $\bar{S}$ .

The other settings used in the MBO framework were: the maximum number of surrogate evaluation to maximise the expected improvement using Bi-POP-CMA-ES was set to  $12000n$ , the reference point  $\mathbf{l} = (l_1, l_2)$  to compute the hypervolume was dynamically determined with  $l_i = \max_{\mathbf{d} \in D} f_i(\mathbf{d}) + 0.1(\max_{\mathbf{d} \in D} f_i(\mathbf{d}) - \min_{\mathbf{d} \in D} f_i(\mathbf{d}))$ , and the overall budget on the number of CFD evaluations was limited to 400.

<sup>2</sup>Python code for the MBO framework is available at: <http://bitbucket.org/arahat/gecco-2017>

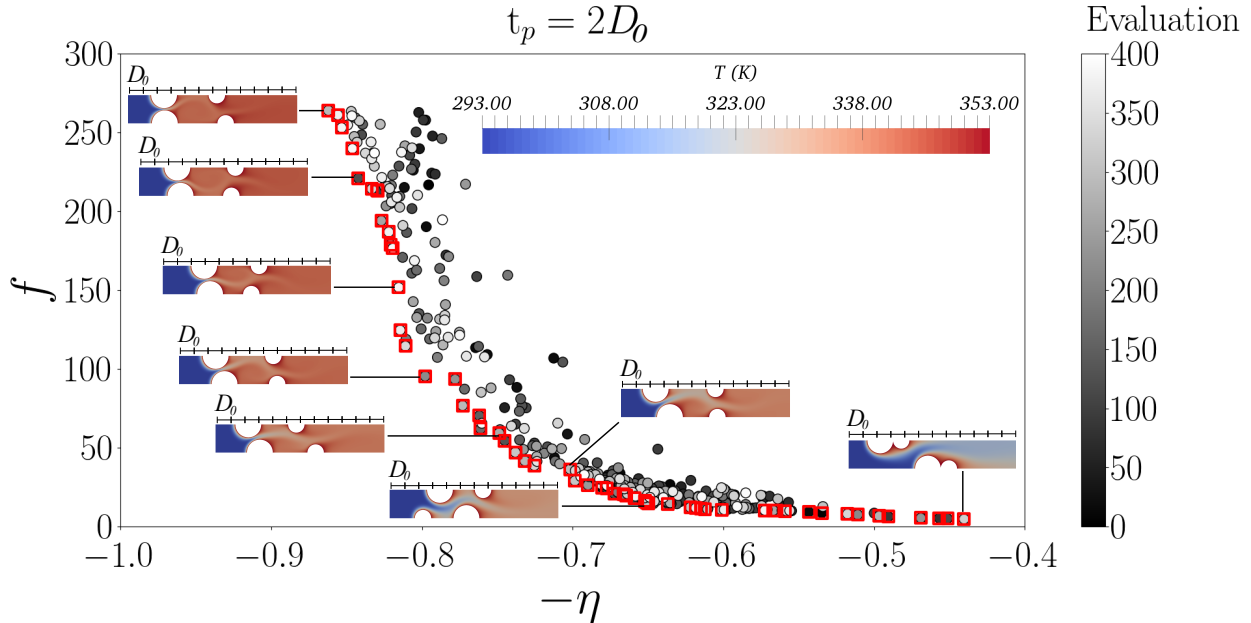


Figure 5: Objective space of the two cost functions (Eqs.9 and 10) with the Pareto front (red squares) and associated tube-bundle heat exchanger designs.

Fig.5 shows the objective space, and the resulting Pareto front (indicated by red-squares). The data points are coloured according to the evaluation number during the optimisation process (grey scale). It can be seen that the majority of solutions at the Pareto front were obtained after 250 evaluations; some of the solutions at the higher values of hydraulic resistance ( $f > 250$ ) were obtained around 350 evaluations. Compared to the equivalent use of GAs (e.g. [15], 140,000 evaluations) shows that the use of Multi-Objective Bayesian Optimisation is considerably more efficient. Some of the geometries (and temperature flowfield) belonging to the Pareto front have been included. Consistently, along the Pareto front, 2 pipes per column provided the best trade-off between the pressure drop, and total heat transfer. For higher values of both objectives (top-left of Fig.5), the distribution of pipes consistently consist of two rows of pipes - the first row having a larger diameter ( $\sim 1.25D_0$ ) than the base, the second with a smaller diameter ( $\sim 0.5D_0$ ). The position of these pipes form a similar pattern to an in-line formation; it can be seen there is a slight offset between the two rows - allowing to correct the flow for a uniform outflow ( $u_{out}$ ). As the pressure-drop decreases the offset between the front two pipes increases, reducing the local Reynolds number between them, and allowing for a more effective pressure recovery; once again, the smaller pipes in the wake of these are positioned to increase the streamwise velocity component. For smaller values of total heat transfer ( $\eta < 0.7$ ) the pipe formation takes on a more staggered distribution, with the center of at the opposite column being outside than the radius of the pipe on the first column. As the total heat transfer continues to decrease (with marginal changes to the pressure drop), the pipes begin to combine for each column, i.e. the longitudinal distance between smaller pipe in the wake of the larger one begins to reduce. Finally, the configuration with the lowest pressure drop and total heat transfer (bottom-right of the Fig.5) shows a staggered configuration but with a smaller pipe in the pipe directly behind the larger one; as discussed earlier, such a configuration has proven to be effective for reducing frictional losses across the heat exchanger (e.g. [7]), but, in the present work, shows that this also reduces the heat transfer.

## 6 Conclusions and Future Work

In this study, Multi-objective Bayesian Optimisation has been applied to a two-dimensional tube bundle heat exchanger, with the aim of optimising the radii, number, and pitch ratios of the tubes. The cost functions (objectives) of this problem were to minimise the frictional losses (pressure drop) and maximise the total heat transfer across the apparatus. All evaluations rely on accurate CFD simulations for each evaluation,

after having checked mesh independency and avoiding any undue influence of the boundary conditions on the cost functions. Accepting a relatively small number of evaluations (400) to that of GAs (often applied in the literature), the Pareto front connecting the equivalent hydraulic resistance and efficiency of heat transfer were obtained. The resulting Pareto front consists of designs shows a consistent use of two pipes in tandem per column. For higher hydraulic resistance (and heat transfer), the positions of pipes generally show a pseudo in-line configuration, consisting of larger pipes followed by smaller pipes in the wake. For smaller values of the cost functions, the pipe configurations consist of a staggered formation.

For future work, considering the apparatus considered is a mini-channel tube heat-exchanger, minimising the overall size of the heat exchanger will be considered as third, additional objective function. The transversal pitch,  $t_p$ , will also be considered as a design variable, rather than defined as a constant in the present work; this will allow for the analysis of a compact heat exchanger. Furthermore, as typical heat exchangers operate with flows consisting of Reynolds numbers greater than 1000, the possible impact of turbulence on the findings will also be checked.

### Acknowledgments

This work was supported by the UK Engineering and Physical Sciences Research Council (EPSRC) grant (reference number: EP/M017915/1) for the University of Exeter’s College of Engineering, Mathematics, and Physical Sciences. The CFD simulations were performed on the ISCA HPC in the Advanced Computing Facility in the University of Exeter, UK. 16CPU 2x Intel Haswell E5-2640v3 2.6GHz cores were used.

### References

- [1] K. Park, D-H. Choi, and K-S. Lee. Optimum design of plate heat exchanger with staggered pin arrays. *Numerical Heat Transfer A*, 45:347–361, 2004.
- [2] P. Li and K-Y. Kim. Multiobjective optimization of staggered elliptical pin-fin arrays. *Numerical Heat Transfer A*, 53:418–431, 2008.
- [3] Indraneel Das and John E Dennis. A closer look at drawbacks of minimizing weighted sums of objectives for pareto set generation in multicriteria optimization problems. *Structural optimization*, 14(1):63–69, 1997.
- [4] E. Konstantinidis, S. Balabani, and M. Yianneskis. Relationship between vortex shedding lock-on and heat transfer. *Chemical Engineering Research and Design*, 81(6):695–699, 2003.
- [5] E. Konstantinidis, D. Castiglia, and S. Balabani. An experimental study of steady and pulsating cross-flow over a semi-staggered tube bundle. *Chemical Engineering Research and Design*, 219(3), 2005.
- [6] D. Traub. Turbulent heat transfer and pressure drop in plain tube bundles. *Chemical Engineering and Processing: Process Intensification*, 28(3):173–181, 1990.
- [7] D. Bacellar, A. Vikrant, Z. Huang, and R. Radermacher. Airside friction and heat transfer characteristics for staggered tube bundle in crossflow configuration with diameters from 0.5mm to 2.0mm. *International Journal of Heat and Mass Transfer*, 98:448–454, 2016.
- [8] A. Bejan and A. Fowler. The optimal spacing between horizontal cylinders in a fixed volume cooled by natural convection. *International Journal of Heat and Mass Transfer*, 38(11):2047–2055, 1995.
- [9] G. Stanescu, A. Fowler, and A. Bejan. The optimal spacing of cylinders in free-stream cross-flow forced convection. *International Journal of Heat and Mass Transfer*, 39(2):311–317, 1996.
- [10] R. Matos, J. Vargas, T. Laursen, and F. Saboya. Optimization study and heat transfer comparison of staggered circular and elliptic tubes in forced convection. *International Journal of Heat and Mass Transfer*, 44:3953–3961, 2001.
- [11] R. Matos, J. Vargas, T. Laursen, and A. Bejan. Optimally staggered finned circular and elliptic tubes in forced convection. *International Journal of Heat and Mass Transfer*, 47:1347–1359, 2004.
- [12] R. Matos, T. Laursen, J. Vargas, and A. Bejan. Three-dimensional optimization of staggered finned circular and elliptic tubes in forced convection. *International Journal of Thermal Sciences*, 43:477–487, 2004.
- [13] R. Hilbert, G. Janiga, R. Baron, and D. Thevenin. Multi-objective shape optimization of a heat

- exchanger using parallel genetic algorithms. *International Journal of Heat and Mass Transfer*, 49:2567–2577, 2006.
- [14] P. Ranuta, G. Janigab, E. Nobilea, and D. Thevenin. Multi-objective shape optimization of a tube bundle in cross-flow. *International Journal of Heat and Mass Transfer*, 68:585–598, 2014.
- [15] L. Daroczy, G. Janiga, and D. Thevenin. Systematic analysis of the heat exchanger arrangement problem using multi-objective optimization. *Energy*, 65:364–373, 2014.
- [16] Y. Ge, Z. Liu, F. Shan, F. Yuan, R. Long, and W. Liu. Multi-objective arrangement optimization of a tube bundle in cross-flow using cfd and genetic algorithm. In *9th International Conference on Applied Energy, ICAE2017*, 9th International Conference on Applied Energy, ICAE2017, pages 21–24, 2007.
- [17] L. Gu, J. Min, X. Wu, and L Yang. Airside heat transfer and pressure loss characteristics of bare and finned tube heat exchangers used for aero engine cooling considering variable air properties. *International Journal of Heat and Mass Transfer*, 108:1839–1849, 2017.
- [18] T-S. Wung and C.J. Chen. Finite analytic solution of convective heat transfer for tube arrays in crossflow: Part i—flow field analysis. *Journal of Heat Transfer*, 111(3):633–640, 1989.
- [19] S. Aiba, H. Tsuchida, and T. Ota. Heat transfer around a tube in a bank. *Bulletin of JSME*, 24(188):380–387, 1981.
- [20] S. Aiba, H. Tsuchida, and T. Ota. Heat transfer around tubes in in-line tube banks. *Bulletin of JSME*, 25(204):919–926, 1982.
- [21] S. Benhamadouche and D. Laurence. Les, coarse les, and transient rans comparisons on the flow across a tube bundle. *International Journal of Heat and Fluid Flow*, 24:470–479, 2003.
- [22] H. Iacovides, B. Launder, and A. West. A comparison and assessment of approaches for modelling flow over in-line tube banks. *Journal of Heat Transfer*, 49:69–79, 2014.
- [23] A. Zukauskas and R. Ulinskas. *Heat transfer from tubes in crossflow*. Hemisphere, Washington, DC, 1988.
- [24] W.A. Khan, J.R. Culham, and M.M. Yovanovich. Convection heat transfer from tube banks in crossflow: Analytical approach. *International Journal of Numerical Methods for Heat and Fluid Flow*, 49:4831–4838, 2006.
- [25] Y. Wang, X. Gu, Z. Jin, and K. Wang. Characteristics of heat transfer for tube banks in crossflow and its relation with that in shell-and-tube heat exchangers. *International Journal of Heat and Mass Transfer*, 93:584–594, 2016.
- [26] K. W. Nam, J. H. Jeong, K. S. Kim, and M. Y. Ha. The effects of heat transfer evaluation methods on nusselt number for mini-channel tube bundles. In *2010 3rd International Conference on Thermal Issues in Emerging Technologies Theory and Applications*, pages 361–370, 2010.
- [27] S.G. Mavridou, E. konstandinidis, and D.G. Bouris. Experimental evaluation of pairs of inline tubes of different size as components for heat exchanger tube bundles. *International Journal of Heat and Mass Transfer*, 90:280–290, 2015.
- [28] S.G. Mavridou and D.G. Bouris. Numerical evaluation of a heat exchanger with inline tubes of different size for reduced fouling rates. *International Journal of Heat and Mass Transfer*, 55:5185–5195, 2012.
- [29] D. Barkley and R.D. Henderson. Three-dimensional floquet stability analysis of the wake of a circular cylinder. *Journal of Fluid Mechanics*, 322:215–241, 1996.
- [30] C. Norberg. An experimental investigation of the flow around a circular cylinder: influence of aspect ratio. *Journal of Fluid Mechanics*, 258:287–316, 1996.
- [31] Henry G Weller, G Tabor, Hrvoje Jasak, and C Fureby. A tensorial approach to computational continuum mechanics using object-oriented techniques. *Computers in physics*, 12(6):620–631, 1998.
- [32] S.V Patankar and D.B Spalding. A calculation procedure for heat, mass and momentum transfer in three-dimensional parabolic flows. *International Journal of Heat and Mass Transfer*, 15(10):1787 – 1806, 1972.
- [33] A. Lemouedda, M. Breuer, E. Franz, T. Botsch, and A. Delgado. Optimization of the angle of attack of delta-winglet vortex generators in a plate-fin-and-tube heat exchanger. *International Journal of Heat and Mass Transfer*, 53(23):5386–5399, 2010.
- [34] E. Nobile, F. Pinto, and G. Rizzetto. Geometric parameterization and multiobjective shape optimization of convective periodic channels. *Numerical Heat Transfer, Part B: Fundamentals An International Journal of Computation and Methodology*, 50(5):425–453, 2006.
- [35] D. Copiello and G. Fabbri. Multi-objective genetic optimization of the heat transfer from longitudinal

- wavy fins. *International Journal of Heat and Mass Transfer*, 52(5-6):1167–1176, 2009.
- [36] S. Baodong, W. Lifeng, L. Jianyun, and C. Heming. Multi-objective optimization design of a micro-channel heat sink using adaptive genetic algorithm. *International Journal of Numerical Methods for Heat and Fluid Flow*, 21(3):353–364, 2011.
- [37] Z. Iqbal, K. Syed, and M. Ishaq. Optimal convective heat transfer in double pipe with parabolic fins. *International Journal of Heat and Mass Transfer*, 54(25-26):5415–5426, 2011.
- [38] X. Cheng. Entropy resistance minimization: an alternative method for heat exchanger analyses. *Energy*, 58:672–678, 2013.
- [39] S-H Yu., K-S Lee., and S-J Yook. Optimum design of a radial heat sink under natural convection. *International Journal of Heat and Mass Transfer*, 54(11-12):2499–2505, 2011.
- [40] B. Pussoli, J. Barbosa Jr, L. Da Silva, and M. Kaviani. Optimization of peripheral finned-tube evaporators using entropy generation minimization. *International Journal of Heat and Mass Transfer*, 55(25-26):7838–7846, 2012.
- [41] S.J. Daniels, A.A.M. Rahat, R.M. Everson, G.R. Tabor, and J.E. Fieldsend. A suite of computationally expensive shape optimisation problems using computational fluid dynamics. In *15th International Conference on Parallel Problem Solving from Nature, PPSN2018*, 15th International Conference on Parallel Problem Solving from Nature, PPSN2018, 2018.
- [42] B.N. Rajani, H.G. Lanka, and S. Majumdar. Laminar flow past a circular cylinder at reynolds number varying from 50 to 5000. Technical report, National Aerospace Laboratories, Bangalore, India, 2005.
- [43] B.N. Rajani, A. Kandasamy, and S. Majumda. Numerical simulation of laminar flow past a circular cylinder. *International Journal of Heat and Mass Transfer*, 33(3):1228–1247, 2009.
- [44] George B Arfken, Hans J Weber, and Frank E Harris. *Mathematical methods for physicists: a comprehensive guide*. Academic press, 2011.
- [45] Carlos A. Coello Coello, Gary B. Lamont, and David A. Van Veldhuizen. *Evolutionary Algorithms for Solving Multi-Objective Problems*. Springer, 2007.
- [46] Alma A. M. Rahat, Richard M. Everson, and Jonathan E. Fieldsend. Alternative infill strategies for expensive multi-objective optimisation. In *Proceedings of the Genetic and Evolutionary Computation Conference, GECCO '17*, pages 873–880, New York, NY, USA, 2017. ACM.
- [47] B. Shahriari, K. Swersky, Z. Wang, R.P. Adams, and N. de Freitas. Taking the human out of the loop: A review of bayesian optimisation. In *Proceedings of the IEEE*, volume 104, pages 148–175, 2016.
- [48] E. Zitzler. *Evolutionary algorithms for multiobjective optimization: Methods and applications*. PhD thesis, 1999.
- [49] M. Fleischer. The measure of pareto optima applications to multi-objective metaheuristics. In *International Conference on Evolutionary Multi-Criterion Optimization*, pages 519–533. Springer, 2003.
- [50] M. D. McKay, R. J. Beckman, and W. J. Conover. A comparison of three methods for selecting values of input variables in the analysis of output from a computer code. *Technometrics*, 42(1):55–61, 2000.
- [51] N. Hansen. Benchmarking a BI-population CMA-ES on the BBOB-2009 function testbed. In *Proceedings of the 11th Annual Conference Companion on Genetic and Evolutionary Computation Conference: Late Breaking Papers, 2389–2396*, 2009.
- [52] Donald R Jones, Matthias Schonlau, and William J Welch. Efficient global optimization of expensive black-box functions. *Journal of Global Optimization*, 13(4):455–492, 1998.